Enhanced Estimation of Thermodynamic Parameters: A Hybrid Approach Integrating Rough Set Theory and Deep Learning

Man Zhang[1, 2]

[1] College of Economics and Management, Nanjing University of Aeronautics and Astronautics, Nanjing 210016, China
[2] Business School, Northwest University of Political Science and Law, Xi'an 710122, China

Corresponding Author Email: 20060127@nwupl.edu.cn

ABSTRACT

In contemporary industrial processes, the estimation of thermodynamic parameters is paramount, yet challenging due to the impact of diverse variables. These parameters, often elusive, require precise identification through computational models. Recently, both deep learning and rough set theory have emerged as powerful tools in various domains. This study proposes a novel approach that synergizes these two methodologies for the enhanced estimation of thermodynamic parameters. The focus lies on developing a one-dimensional, multi-regional coupled temperature field model, alongside the identification of pertinent thermodynamic parameters. The integration of deep learning with rough set theory forms the crux of this methodology, aiming to address the challenges in processing ambiguous and uncertain data, and in managing high-dimensional, complex structures. The hybrid model thus constructed is poised to significantly improve the handling of ambiguous and uncertain information, thereby boosting the accuracy and efficiency in identifying thermodynamic parameters. The methodological advancement presented in this study not only contributes to the field of thermodynamic parameter estimation but also sets a precedent in the application of integrated computational techniques.

1. INTRODUCTION

The precise estimation of thermodynamic parameters is recognized as critical in modern industrial production, crucial for system stability, energy efficiency optimization, pollution reduction, and economic benefit enhancement [1-3]. The complexity of industrial processes, compounded by the interplay of environmental conditions, material properties, and equipment parameters, often renders direct observation and measurement of these parameters a formidable challenge [4-7]. Hence, the development of a reliable and accurate model for thermodynamic parameter identification and estimation holds significant theoretical and practical importance in the realm of industrial process optimization [8, 9].

Recent advancements in deep learning, a sophisticated subset of machine learning technologies, have spurred unprecedented achievements in areas like image recognition, natural language processing, and predictive analytics, offering novel perspectives and methodologies for tackling intricate issues [10-13]. Concurrently, rough set theory, renowned for its efficacy in data analysis and knowledge acquisition, has gained recognition for its proficiency in managing uncertainty and ambiguity, demonstrating exceptional utility in diverse complex problem-solving contexts [14-16]. The integration of these two methodologies, deep learning and rough set theory, in thermodynamic parameter identification, promises to harness the strengths of both, thereby enhancing the accuracy and reliability of the identification process, and presenting wide-ranging application prospects and substantial theoretical contributions.

However, current approaches in thermodynamic parameter identification, deep learning, and rough set theory exhibit significant limitations [17-19]. Predominantly, these methodologies grapple with the processing of ambiguous and uncertain information and struggle with complex, high-dimensional data structures, which crucially impacts the precision and reliability of identification outcomes. These shortcomings present substantial barriers to the optimization of industrial production processes [20-22].

In light of these challenges, this paper introduces a novel methodological approach: the amalgamation of deep learning and rough set theory for thermodynamic parameter identification. The key research focuses include the establishment of a one-dimensional multi-regional coupled temperature field model for thermodynamic parameter identification, and the construction of a composite model that integrates deep learning with rough set theory. This innovative approach is anticipated to adeptly manage ambiguous and uncertain information, thereby elevating the precision and efficiency of thermodynamic parameter identification. Such advancements are poised to offer invaluable theoretical and practical guidance in industrial production process optimization, specifically in the accurate estimation of thermodynamic parameters.

2. MODEL DESCRIPTION AND THERMODYNAMIC PARAMETER IDENTIFICATION

2.1 Model description

Temperature fields experiencing predominant heat conduction in vertical planes are observed in diverse natural and artificial environments. For example, the Earth's crust is composed of multiple strata, transitioning in temperature from cooler surface layers to warmer depths. Similarly, atmospheric temperatures vary with altitude, decreasing in the troposphere and increasing in the stratosphere. In aquatic environments like lakes and oceans, temperature changes with depth, generally warmer at the surface and cooler below. In built environments, such as high-rise buildings, temperature gradients are often observed from lower to upper floors.

The analysis of these temperature fields is instrumental in understanding climatic systems, contributing to more accurate climate change predictions and responses. In architectural contexts, it aids in efficient energy management. In aquatic ecosystems, such temperature variations are crucial for the survival of species and ecosystem stability, thus facilitating environmental protection. Geologically, these temperature distributions inform the exploitation of geothermal resources and the understanding of crustal dynamics.

In vertical temperature fields, a thermal gradient typically emerges with depth or altitude due to heat transfer mechanisms like conduction, convection, and radiation, transferring heat from warmer to cooler areas. Given the complexity of these fields, models often simplify by focusing predominantly on vertical heat conduction, a valid assumption in many cases due to its predominance over horizontal transfer in both natural and man-made environments.

For modeling these multi-layer temperature fields, a Cartesian coordinate system is employed. This entails selecting a point on the top two material layers' interface as the origin, extending a vertical line downwards to form the z-axis. Consequently, a right-angled coordinate system is established, with the interface as the origin and the vertical direction as the z-axis.

Consider a three-layered temperature field with layer thicknesses denoted by m_1, m_2, and m_3. The respective regions of these materials are represented as $F_1 = [-m_1, 0]$, $F_2 = [0, -m_2]$, and $F_3 = [m_2, m_2 + m_3]$. The comprehensive time domain for the coupled temperature field is designated as $U = [0, y_d] \subset E$.

$$F = F_1 \cup F_2 \cup F_3 \subset E, W = F \times U \subset E^2,$$
$$W_k = F_k \times U \subset E^2, k = 1, 2, 3. \tag{1}$$

The energy conservation principle, a cornerstone in thermodynamics, dictates that energy within a closed system is conserved, merely transforming from one form to another. Fourier's law of heat conduction, a fundamental tenet in this context, posits that the flow density of heat is directly proportional to the temperature gradient, the proportionality constant being the thermal conductivity of the material. Under these guiding principles, a multi-layer temperature field equation is constructed. This equation reflects the principle that the temporal rate of temperature change is equal to the product of thermal diffusivity and the spatial second-order derivative of temperature, encapsulating the characteristic of heat migration from warmer to cooler areas. In alignment with this model, specific boundary conditions are delineated. The

initial conditions are defined as the temperature distribution at time $t=0$, and the boundary conditions dictate the temperature or heat flow at the spatial perimeters of the system. The heat source term is symbolized by $h(x, y)$, the heat exchange coefficient between the uppermost and the subsequent material layer is denoted by g, and the temperature of the topmost layer is represented by Y_v. Thus, the function $g_0(y)$ is described as $g_0(y) = (g(Y(x, y) - Y_v/J_a)_{x=-m1}$, setting the parameters for heat exchange at the uppermost boundary.

$$\begin{cases} (v\vartheta)(x, y)\dfrac{\partial Y(x, y)}{\partial y} = \dfrac{\partial}{\partial x}\left(J(x, y)\dfrac{\partial Y(x, y)}{\partial x}\right) \\ \quad + h(x, y), (x, y) \in F \times U \\ Y(x, 0) = Y_0(x), x \in F \\ \dfrac{\partial Y(x, y)}{\partial x}\bigg|_{x=-m_1} = g_0(y), y \in U \\ Y(x, y)\big|_{x=m_2+m_3} = Y_3(y), y \in U \end{cases} \tag{2}$$

In multi-layer temperature fields, the material constituting the bottom layer is typically characterized by high thermal conductivity, significant density, and substantial specific heat capacity. These attributes are pivotal in facilitating effective heat transfer and regulation within the temperature field, thereby contributing to its stability. Further, the density of the material $x \in F_2$ in the bottom layer, is signified by $A_u(x)$. The three layers in the temperature field are characterized by their average specific heats, densities, and thermal conductivities, denoted by v_a, ϑ_a, J_a, v_u, ϑ_u, J_u, v_q, ϑ_q, J_q, respectively. An approximate formula for these calculations is presented, facilitating the estimation of these parameters.

$$A_u(x) = \begin{cases} 14.24 - 19.39x, 0 < x \le 0.57l \\ 3.2, 0.57l < x \le m_2 \end{cases} \tag{3}$$

Constants in the model are represented by v_a, ϑ_a, J_a, v_q, ϑ_q, and J_q. The vector comprising parameters to be identified is expressed as $w = (v_u, \vartheta_u, J_u)$, clearly situated within the mathematical domain E^3_+. The subsequent equations and derivations follow, providing a framework for the precise estimation of these thermodynamic parameters within the defined system.

$$(v\vartheta)(x, y) = \begin{cases} v_a\vartheta_a, (x, y) \in W_1 \\ v_u\vartheta_u, (x, y) \in W_2 \\ v_q\vartheta_q, (x, y) \in W_3 \end{cases} \tag{4}$$

$$J(x, y) = \begin{cases} J_a, (x, y) \in W_1 \\ J_u, (x, y) \in W_2 \\ J_q, (.x, y) \in W_3 \end{cases} \tag{5}$$

The empirical determination of the parameter w within the domain E^3_+ necessitates the establishment of its lower and upper bounds. The lower bound of the measured parameter w is denoted as $w_- \in E^3_+$, and the upper bound is represented as $w_+ \in E^3_+$. This delineation allows for the formulation of the

permissible range of the parameter w, vital for the model's calibration and validation.

$$W_{sf} = \{w : w_- \leq w \leq w_+\} \in E_+^3 \qquad (6)$$

The influence of solar radiation on the temperature field, particularly the shortwave radiation from the sun, is a fundamental aspect of the model. The intensity and angle of solar radiation play a pivotal role in shaping the temperature field, with intense solar radiation elevating temperatures in the upper layer and consequently affecting the lower layers. The angle at which solar radiation strikes influences its intensity and distribution, further impacting the temperature field. The interaction of solar radiation with materials, characterized by their reflectivity, transmissivity, and extinction coefficient, dictates the proportion of radiation that is reflected, absorbed, and transmitted. In the model, the shortwave radiation from the sun, combined with the reflectivity, transmissivity, and extinction coefficient of the middle layer, is expressed through the variables ε_k, β_k, U_{pk}, and e_k. The heat source term $h(x, y)$, encompassing the effect of solar radiation on the temperature field, is characterized by the following expression:

$$h(x, y) = \begin{cases} h_1(x, y), (x, y) \in W_1 \\ h_2(x, y), (x, y) \in W_2 \\ 0, (x, y) \in W_3 \end{cases} \qquad (7)$$

where,

$$h_k(x, y) = \varepsilon_k (1 - \beta_k) e_k U_{pk} \exp(-e_k |x|), k = 1, 2. \qquad (8)$$

2.2 Identification of thermodynamic parameters

The atmospheric layer is utilized as a model to explore the characteristics of a multi-layer temperature field and the interrelationships among its layers. Observational projects in this context include the measurement of temperatures at various altitudes, barometric pressure readings at different elevations, humidity levels across layers, wind speed and direction per layer, shortwave and longwave solar radiation, cloud coverage and precipitation, atmospheric gas composition, aerosol distribution, surface characteristics of the Earth, and atmospheric stability. The subsequent paragraphs delineate the steps for identifying thermodynamic parameters within a one-dimensional multi-layer coupled temperature field model.

Temperature data, spanning various altitudinal layers within the environment, are systematically gathered. The acquisition of this data is predominantly conducted through instruments such as temperature sensors, meteorological stations, and satellites equipped for meteorological observation. Following the collection phase, a pivotal step involves the development of temperature distribution functions. These functions are formulated based on the empirical data's distribution characteristics, ensuring a comprehensive representation of critical influencing factors on temperature, notably altitude, latitude, or temporal aspects. Temperatures at time instance $y_k \in U$ and location $x_j \in F$ are recorded and represented as $Y_f(x_j, y)$, for $k = 1, 2, ..., m_1$, and $j = 1, 2, ... m_x$. Based on the gathered data set $\{Y_f(x_j, y_k)\}$, a temperature distribution function $Y_f(x, y)$, where $(x, y) \in F$, is fitted. The continuity of temperature changes necessitates the assumption of the function $Y_f(x, y) : W \rightarrow E$ being continuous.

In the coupled multi-layer temperature field system, the temperature $Y(x, y; w)$, where $w \in W_{sf}$, is uniquely ascertainable. Post derivation of the temperature distribution function, its accuracy is assessed. The primary metric for this evaluation is the discrepancy between the temperatures determined by the system $Y_f(x, y; w)$ and the empirically measured temperatures $Y_f(x, y)$. The study advances by considering the sum of the squares of these errors as a quadratic functional $K( )$, with the aim to find a temperature distribution function that minimizes this functional, a process known as the least squares estimation.

$$K(w) = \|Y(x, y; w) - Y_f(x, y)\|_{V(W, E)}^2 \qquad (9)$$

Upon formulating the error functional, an identification model is constructed. The purpose of this model is to ascertain a set of thermodynamic parameters that minimizes the error functional. Parameters such as thermal conductivity, density, and specific heat capacity are considered. The identification process involves solving an optimization problem to determine parameters that minimize the error functional within established constraints.

$$SBMX : MIN\ K(w) \quad s.t. \quad Y(x, y : w) \in A \quad w \in W_{sf} \qquad (10)$$

The continuity of the mapping $w \rightarrow Y(x, y; w)$：$W_{sf} \rightarrow A$, along with the functional $K(w)$, relative to the parameter $w \in W_{sf}$, establishes that $W_{sf} \subset E_+^3$ constitutes a non-empty, bounded, and closed set. Consequently, it is deduced that there exists at least one parameter $w^* \in W_{sf}$ that satisfies the following criterion:

$$K(w^*) \leq K(w), \forall w \in W_{sf} \qquad (11)$$

In addressing the optimization problem, a critical analysis of the conditions requisite for achieving an optimal solution is conducted. Fundamental principles of calculus dictate that at a point where a function reaches an extremum, the gradient at this juncture is required to be zero. For the optimal determination of parameter w^*, the standard approach involves computing the first variation of $K(w)$ within the vicinity of w^*. Should $Y(x, y; w)$ be $Ga\hat{t}eaux$ differentiable at $w^* \in W_{sf}$, and $Y'(w^*)$ represent its $Ga\hat{t}eaux$ derivative at $w = w^*$, then $K(w)$ is also deemed $Ga\hat{t}eaux$ differentiable at $w = w^*$. The $Ga\hat{t}eaux$ derivative of $K(w)$ is assumed to be indicated by $Y'(w^*)$, leading to the expression of the necessary condition for optimality regarding w^*:

$$K'(w^*)(w - w^*) \geq 0, \forall w \in W_{sf} \qquad (12)$$

The $Ga\hat{t}eaux$ differentiability of $Y(x, y; h)$ with respect to w at $w = w^*$ is demonstrable. Therefore, the following relation is derived:

$$K_f(w) = \sum_{j=1}^{m_x} \sum_{k=1}^{m_u} \left(Y(x_j, y_k; w) - Y_f(x_j, y_k) \right)^2 \qquad (13)$$

In cases where the computational complexity of the model proves to be exceptionally high, it is pragmatic to employ

approximation methods to simplify the model. The modified identification model, incorporating such simplifications, is then presented as:

$$SBMX_f : MINK_f(w) \quad a.y. \quad Y(x, y; w) \in A \quad w \in W_{sf} \quad (14)$$

## 3. CONSTRUCTION OF AN INTEGRATED ROUGH SET AND DEEP LEARNING MODEL

This research introduces a novel fuzzy rough convolutional neural network (CNN) model, blending fuzzy rough set theory with deep convolutional networks, to effectively identify thermodynamic parameters in a one-dimensional multi-layer coupled temperature field. The model's architecture, illustrated in Figure 1, encompasses several layers: an input layer, convolutional layers, pooling layers, fully connected layers, a fuzzy rough set theory layer, and an output layer. The initial stage involves leveraging the advanced feature-learning capabilities of deep convolutional networks for automated feature extraction from the one-dimensional multi-layer coupled temperature field data. Convolutional layers, employing multiple kernels, convolve the input data to extract local spatial features. Subsequently, pooling layers down sample these features, thereby reducing data dimensions and increasing the model's resilience to minor spatial variations. Fully connected layers further process these high-dimensional feature maps into one-dimensional feature vectors, setting the stage for classification tasks.
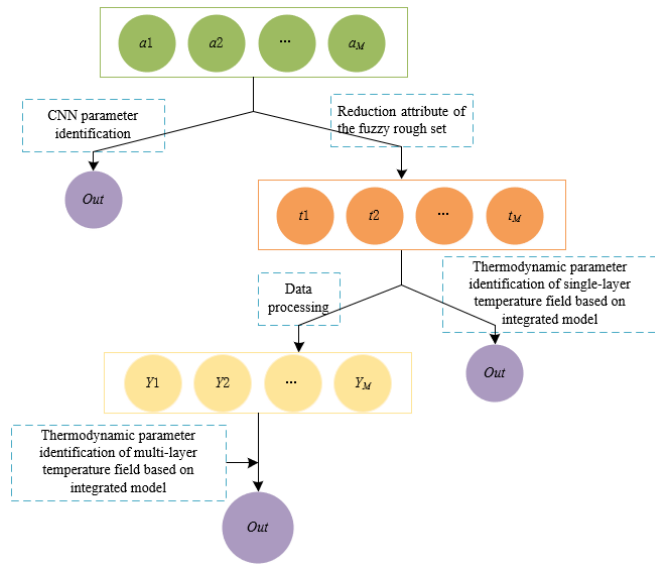

Figure 1. Thermodynamic parameter identification process flowchart

Following the fully connected layers, a layer based on fuzzy rough set theory is integrated. This theory, adept at handling imprecise, uncertain, and fuzzy data, maps the feature vectors into the domain of thermodynamic parameters, thereby enhancing the accuracy of the model's output in reflecting actual parameters. During this phase, the minimization of fuzzy classification uncertainty is pursued as an optimization objective. A differentiable fuzzy rough loss function is proposed to achieve this. Through the optimization of this loss function, the model learns to distinguish more effectively between varying thermodynamic parameters. The final stage

involves computing the derivative of the fuzzy rough loss function and employing the backpropagation algorithm for updating the model's parameters, a crucial step in model training. This iterative process of forward and backward propagation gradually refines the model parameters, aligning the model's predictions more closely with the actual thermodynamic parameters. In this fuzzy rough CNN model, the primary input features include temperature, pressure, humidity data, and other physical parameters pertinent to the one-dimensional multi-layer coupled temperature field. Data sources include ground meteorological stations, meteorological satellites, radar detection systems, and other relevant technologies. Figures 2 and 3 provide schematic representations of the training phase and the fuzzy decision-making phase of the model, respectively.
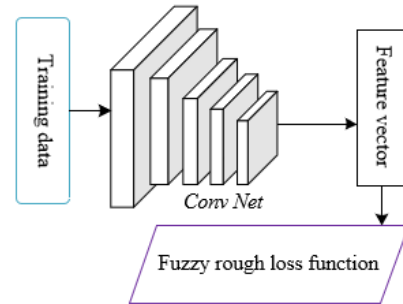
**Figure 2.** Schematic of the training phase of the fuzzy rough CNN model
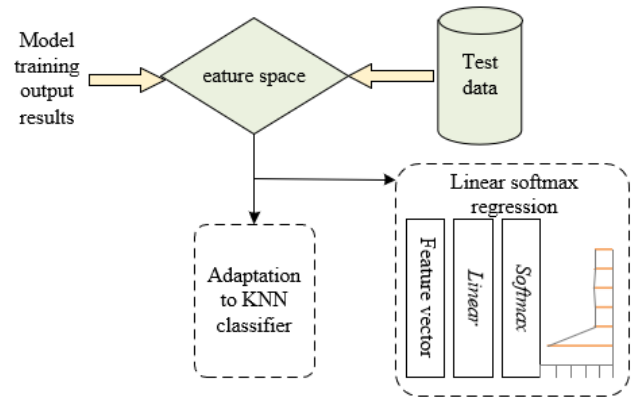
Figure 3. Schematic of the fuzzy decision-making phase of the fuzzy rough CNN

Fuzzy rough set theory, recognized for its efficacy in managing data characterized by uncertainty and fuzziness, plays a pivotal role in the proposed model. Utilizing fuzzy upper and lower approximations, this theory establishes the maximum and minimum bounds within which thermodynamic parameters can range. The disparity between these bounds is utilized to assess the discriminative capability of features in relation to thermodynamic parameters. Consequently, the fuzzy rough loss function, founded on this principle, is formulated. The magnitude of this loss function, indicative of the difference between fuzzy upper and lower approximations, serves as a measure of the features' discriminative power concerning thermodynamic parameters. A smaller value of this function signifies a stronger discriminative ability, enhancing the predictive accuracy of the model. Therefore, the model's optimization objective is to minimize the fuzzy rough

loss function. Figure 4 illustrates the computational flowchart for this loss function.

The derivative calculation process within the fuzzy rough CNN model is a critical aspect of model optimization. The chain rule of derivatives, a cornerstone of the backpropagation algorithm, is employed for the effective computation of derivatives of the loss function with respect to the model parameters. This is integral in neural networks, where outputs result from a series of intricate, interrelated computations. The chain rule enables the sequential backward calculation of the gradient of the loss function. The fuzzy rough loss function, being a complex function of the model's parameters, necessitates the determination of its derivatives for optimization purposes. The entire computational steps of the fuzzy rough loss function being differentiable, the chain rule is applied to ascertain the gradient of the loss function. The feature layer vector, represented by $z^{(l)}$, the weights of the fully connected layer by $q^{(l)}$, and the biases of the fully connected layer by $n^{(l)}$, are considered in this derivation process. The paper exemplifies the derivation of the fuzzy rough loss function $m_{de}(I)$ with respect to $z^{(l)}$, $q^{(l)}$, and $n^{(l)}$.
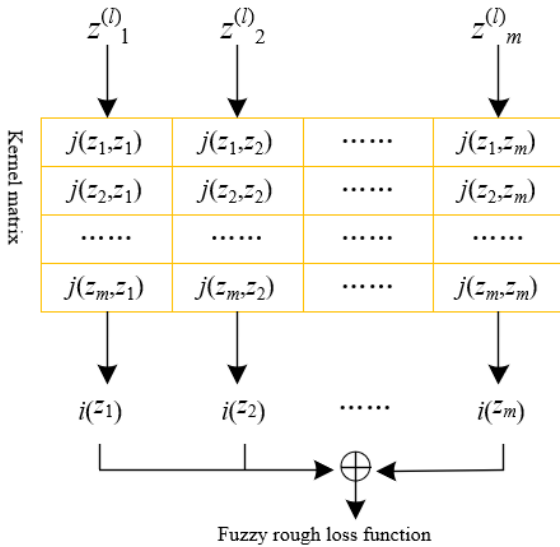
Figure 4. Schematic of the calculation process of the fuzzy rough loss function

The computation of the fuzzy rough loss function derivatives constitutes a crucial step in the model's optimization process. This function, representing the discrepancy between fuzzy upper and lower approximations, undergoes differentiation to calculate its partial derivatives. In accordance with the fundamental theorem of calculus, these partial derivatives are determined as the differences between those of the fuzzy upper and lower approximations. This necessitates the differentiation of the loss function's formula. The partial derivative formulas for $m_{de}(I)$ with respect to $z^{(l)}$, $q^{(l)}$, and $n^{(l)}$ are articulated as follows:

$$\frac{\partial m_{de}(I)}{\partial z^{(l)}} = \sum_{t \in I} \frac{\partial i(t)}{\partial z^{(l)}}$$

$$\frac{\partial m_{de}(I)}{\partial q^{(l)}} = \sum_{t \in I} \frac{\partial m_{de}(I)}{\partial z^{(l)}} \frac{\partial z^{(l)}}{\partial q^{(l)}} \quad (15)$$

$$\frac{\partial m_{de}(I)}{\partial n^{(l)}} = \sum_{t \in I} \frac{\partial m_{de}(I)}{\partial z^{(l)}} \frac{\partial z^{(l)}}{\partial n^{(l)}}$$

For two given samples, denoted by z, $t \in I$, and the feature vector generated for sample t through the "*ConvNet*" represented by $t^{(l)} \in G^{(l)}$, the derivative of the classification uncertainty $i(z)$ of sample z with respect to $t^{(l)}$ is derived through the following formula:

$$\frac{\partial i(z)}{\partial t^{(l)}} = \sum_{f_u \in F} \left(\frac{\partial \overline{j_Y} f_u(z)}{\partial t^{(l)}} - \frac{\partial \underline{j_A} f_u(z)}{\partial t^{(l)}} \right) \quad (16)$$

Subsequently, the fuzzy lower approximation is computed. This approximation, being a function of the sample feature vector, necessitates differentiation of each element of this vector. The complexity of this process is attributed to the fact that the sample feature vector results from a series of intricate calculations, each potentially influenced by other elements or model parameters. For a sample in the training set, represented by z, and $t = arg\ min_{t \in I}((f_u(t)-1)j(z,t)+1)$, the formula for derivation is as follows:

$$\frac{\partial \underline{j_A} f_u(z)}{\partial z^{(l)}} = (f_u(t)-1) \frac{\partial j(z,t)}{\partial z^{(l)}},$$

$$\frac{\partial \underline{j_S} f_u(z)}{\partial t^{(l)}} = (f_u(t)-1) \frac{\partial j(z,t)}{\partial t^{(l)}} \quad (17)$$

The derivation of the fuzzy upper approximation follows a procedure akin to that of the fuzzy lower approximation. Each element of the sample feature vector undergoes differentiation, employing the chain rule of derivatives. The formula for this derivation process is as follows:

$$\frac{\partial \overline{j_Y} f_u(z)}{\partial z^{(l)}} = f_u(t) \frac{\partial j(z,t)}{\partial z^{(l)}},$$

$$\frac{\partial \overline{j_Y} f_u(z)}{\partial t^{(l)}} = f_u(t) \frac{\partial j(z,t)}{\partial t^{(l)}} \quad (18)$$

Subsequently, differentiation of the Gaussian kernel function $j(z, t)$ is undertaken. As a function dependent on the sample feature vector, the Gaussian kernel function requires partial derivatives with respect to these vectors. This step entails differentiating the Gaussian kernel function's formula and applying the chain rule of derivatives. The derivative of $j(z, t)$ with respect to $z^{(l)}$ is expressed by:

$$\frac{\partial r^{-\frac{\left(z^{(l)}-t^{(l)}\right)^2}{\sigma}}}{\partial z^{(l)}} = -\frac{2\left(z^{(l)}-t^{(l)}\right)r^{-\frac{\left(z^{(l)}-t^{(l)}\right)^2}{\sigma}}}{\sigma} \quad (19)$$

Following these steps, the partial derivative $\partial m_{de}(I)/\partial z^{(l)}$ of the fuzzy rough loss function $m_{de}(I)$ in relation to the sample z's feature vector is computable. This derivative emerges as a product of several components: the partial derivatives of the fuzzy rough loss function with respect to both the fuzzy upper and lower approximations, and the partial derivatives of these approximations in relation to the sample feature vector. Assuming the output of the model's last convolutional layer is denoted by $z^{(l-1)}$, the normalized output of the fully connected layer by $z^{(l)}$, the weight matrix by $q^{(l)}$, and the bias vector by $n^{(l)}$, the following relations are established: $x^{(l)}$ is represented as $q^{(l)} \times z^{(l-1)} + n^{(l)}$, and the normalization coefficient α^2_N as $\sum_{z \in}$

$t(q^{(l)} \times z^{(l-1)} + n^{(l)})^2$. Consequently, the output of the fully connected layer is expressed as $z^{(l)} = x^{(l)} / (\alpha^2_N)^{1/2}$. The formulas for deriving $m_{de}(I)$ in relation to α^2_N and $x^{(l)}$ are:

$$\frac{\partial m_{de}(I)}{\partial \alpha^2_N} = \sum_{z \in I} \frac{\partial m_{de}(I)}{\partial z^{(l)}} \left(-\frac{x^{(l)}}{2} \left(\alpha^2_N \right)^{-\frac{3}{2}} \right)$$

$$\frac{\partial m_{de}(I)}{\partial x^{(l)}} = \frac{\partial m_{de}(I)}{\partial z^{(l)}} \frac{1}{\sqrt{\alpha^2_N}} + \frac{\partial m_{de}(I)}{\partial \alpha^2_N} \left(2 \times x^{(l)} \right)$$

(20)

The procedure entails the application of differential calculus to the formulas of the loss function, including both the fuzzy upper and lower approximations. The chain rule of derivatives is methodically employed in this process. Furthermore, for a sample z in the fully connected layer with unnormalized features denoted by $x^{(l)}$, the formulas for calculating $\partial m_{de}(I)/\partial q^{(l)}$ and $\partial m_{de}(I)/\partial n^{(l)}$ using the chain rule of derivatives are:

$$\frac{\partial m_{de}(I)}{\partial q^{(l)}} = \sum_{z \in I} \frac{\partial m_{de}(I)}{\partial x^{(l)}} z^{(l-1)}$$

$$\frac{\partial m_{de}(I)}{\partial n^{(l)}} = \sum_{z \in I} \frac{\partial m_{de}(I)}{\partial x^{(l)}}$$

(21)

$$\frac{\partial m_{de}(I; \varphi)}{\partial \varphi} = \sum_{z \in I} \frac{\partial m_{de}(I)}{\partial x^{(l)}} \frac{\partial x^{(l)}}{\partial \varphi}$$

(22)

4. EXPERIMENTAL RESULTS AND ANALYSIS

The one-dimensional multi-layer coupled temperature field model, as delineated in this study, demonstrates its potential in accurately capturing the dynamics of temperature changes. This is evidenced by the trends observed in Figures 5 and 6, where the congruence of the measured temperatures (depicted by the black line) and computed temperatures (represented by the red line) over time is noticeable. Despite this general consistency, there are instances where discrepancies between the computed and measured temperatures are evident, indicating areas where the model does not perfectly replicate the actual physical phenomena. This paper's model articulates the interlayer coupling relationships and spatial-temporal characteristics of temperature fields. While deviations are present at certain data points, the overall efficacy of the model in predicting temperature trends is affirmed, underscoring its viability for practical application. The model's proficiency is highlighted by: 1) Its accurate reflection of the empirical data trends, validating the appropriateness of the parameter settings and the strategy for temperature field coupling; 2) Its capability to provide proximate real-world temperature estimations at points of divergence, forming a basis for future enhancements through model optimization and parameter adjustments.

An integrated model, merging deep learning with rough set theory for thermodynamic parameter identification, has been developed. Figure 7 illustrates the variations in fuzzy upper and lower approximations across different iteration counts. At the initial stage of model training, with the iteration count at zero, it is observed that the fuzzy upper approximation's value (represented by the blue line) significantly surpasses that of the fuzzy lower approximation (indicated by the red line). This initial disparity suggests a pronounced degree of uncertainty and fuzziness in the model's early predictions of thermodynamic parameters, as evidenced by the substantial gap between the upper and lower approximation boundaries. As iterations progress, a marked decrease in the fuzzy upper approximation is noted, eventually stabilizing and converging with the fuzzy lower approximation. Post 100 iterations, a parallel trend between these two lines is observed, signaling the model's gradual stabilization and the narrowing of the range for thermodynamic parameter identification. This convergence is indicative of reduced uncertainty and fuzziness in the model's predictions. Notably, beyond a certain iteration threshold, the fuzzy lower approximation remains constant, whereas the fuzzy upper approximation declines from 254 to 190 before stabilizing. This trend suggests an emerging consistency in the model's learned features, reflecting an enhanced comprehension of the intrinsic relationships and structures of thermodynamic parameters. In conclusion, after adequate training, the integrated model combining deep learning and rough set theory demonstrates a significant reduction in the uncertainty and fuzziness associated with thermodynamic parameter identification, thereby enhancing the precision and reliability of its predictions. These findings underscore the proposed model's efficacy and highlight the improvement in its predictive stability and reliability, achieved through iterative learning.
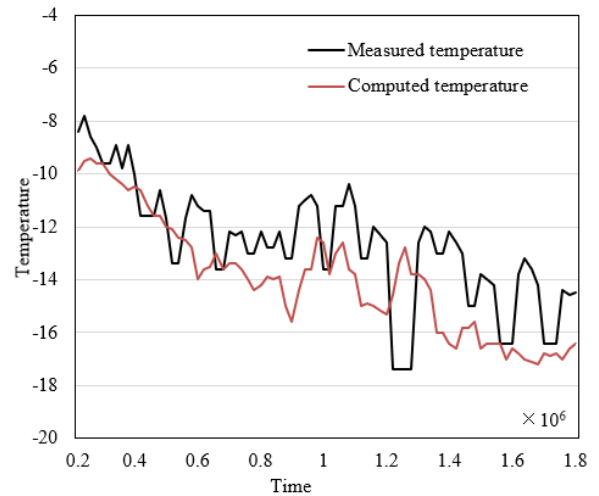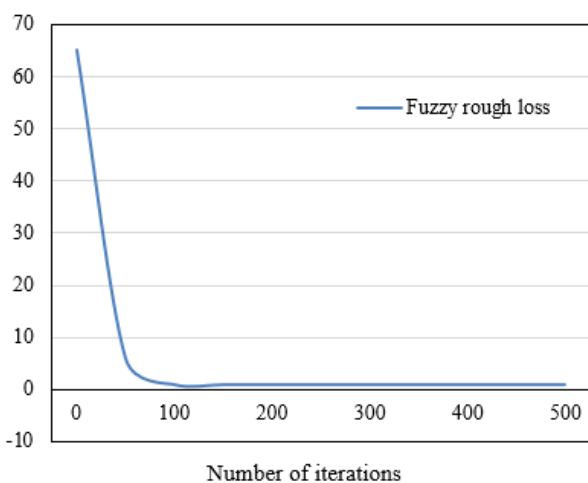
Figure 5. Comparison of computed and measured temperatures for the bottom layer material
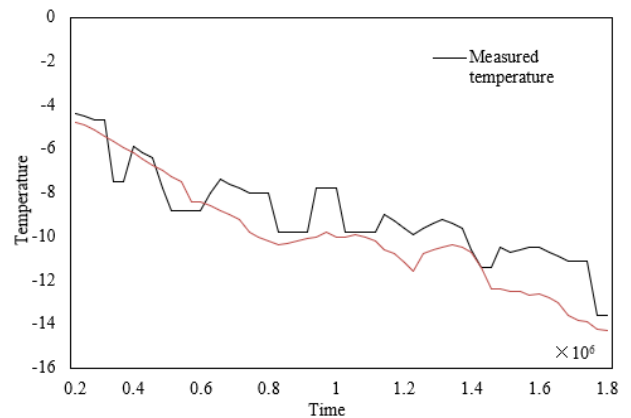
Figure 6. Comparison of computed and measured temperatures for the upper layer material
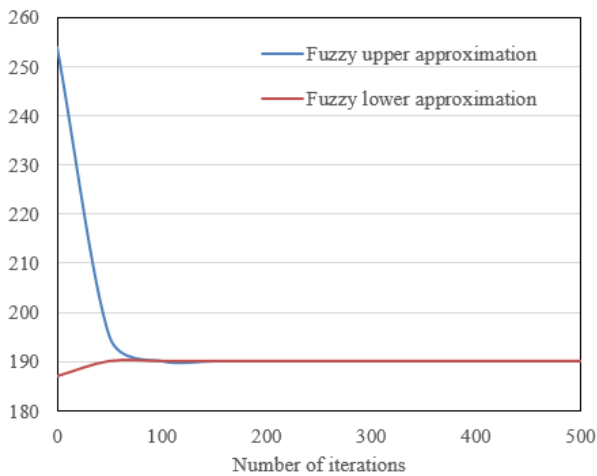
Figure 7. Variation of fuzzy upper and lower approximations with the number of iterations

Figure 8. Variation of fuzzy rough loss function value with the number of iterations

Table 1. Average RMSE in thermodynamic parameter identification for different models

Model	Normal Data	Noise Addition (x)	Missing Features (y)	Missing Samples (z)	$x+y+z$
LSTM	0.1369	0.1258	5.12	0.1326	3.78
FCN	0.1257	0.1289	0.1236	0.1247	0.1274
CNN	0.1236	0.1265	0.7512	0.239	0.6125
The proposed model	0.1216	0.1236	0.1215	0.1205	0.1209

**Table 2.** Average relative error (%) in thermodynamic parameter identification for different models

Model	Normal Data	Noise Addition (x)	Missing Features (y)	Missing Samples (z)	$x+y+z$
LSTM	1.325	1.236	1.358	1.347	1.235
FCN	1.326	1.258	1.458	2.001	3.045
CNN	1.348	1.268	1.356	1.235	1.147
The proposed model	1.125	1.147	1.03	1.147	1.025

Figure 8 provides a graphical representation of the variation in the fuzzy rough loss function value relative to the number of iterations. It is observed that with an increase in iteration counts, the value of the fuzzy rough loss function experiences a marked decline, reaching a state of stability after approximately 100 iterations. This trend signifies that during the initial training phase, the deep learning model rapidly assimilates data features, thereby enhancing the accuracy of thermodynamic parameter estimation. The diminution of the loss function value mirrors the process through which the model refines its predictive precision, assimilating the intrinsic linkages among thermodynamic parameters and the data's distribution characteristics. A diminishing loss function value indicates a reduced disparity between the model's predictions and the actual empirical data. When the loss function value attains and sustains a low, stable level, it suggests that the model has potentially converged to an optimal or near-optimal solution. The results here validate the effectiveness of the proposed model's optimization algorithm, evidencing its applicability and utility in thermodynamic parameter identification.

The data presented in Tables 1 and 2 facilitates a comprehensive comparison of the performance of various models, including the proposed model, Long Short-Term Memory (LSTM), Fully Convolutional Networks (FCN), and CNN, across diverse data conditions. When evaluated on standard datasets (free from noise, missing features, and samples), the proposed model exhibits a lower average Root Mean Square Error (RMSE) and average relative error compared to the LSTM, FCN, and CNN models. This outcome suggests a superior accuracy of the proposed model in the identification of thermodynamic parameters. In scenarios characterized by compromised data quality, such as datasets with noise, missing features, and samples, the proposed model demonstrates remarkable robustness. Particularly notable is its performance in the combined $x+y+z$ condition, where it maintains the lowest RMSE and relative error, markedly surpassing the traditional models. This robustness is crucial for practical applications, as real-world data often encompass various imperfections. Contrastingly, while other models exhibit pronounced performance deterioration under data-deficient conditions, the proposed model consistently maintains low error levels. For example, the CNN model's RMSE rises to 0.7512 in the case of missing features (y) and to 0.6125 in the $x+y+z$ scenario, highlighting the significant resilience of the proposed model with respective values of 0.1215 and 0.1209. In conclusion, the proposed model's consistent performance and robustness across different data quality scenarios significantly emphasize its stability and reliability in diverse dataset conditions. These attributes afford the model a substantial advantage in the accurate identification of thermodynamic parameters, underscoring its practical utility.

Figure 9 illustrates the error curves for various models in thermodynamic parameter identification, delineating each model's performance under different data conditions. The proposed model, as depicted, consistently occupies the lower error regions in all scenarios, notably in normal data and in conditions involving noise addition, missing features, missing samples, and their combination ($x+y+z$). This graphical representation unequivocally demonstrates the proposed model's enhanced precision and robustness in contrast to other models. Under diverse conditions, including complete and impaired data sets, the proposed model's error curve is

expected to display a steady and uniform trajectory. In contrast, other models may exhibit more pronounced fluctuations or abrupt increases in error. Especially in scenarios where data is significantly compromised (e.g., $x+y+z$ condition), the disparity in error between the proposed model and others becomes more evident. The proposed model maintains a consistently low error level, while the error curves of the other models show marked elevation, thereby accentuating the superior adaptability and robustness of the proposed model in handling imperfect data.
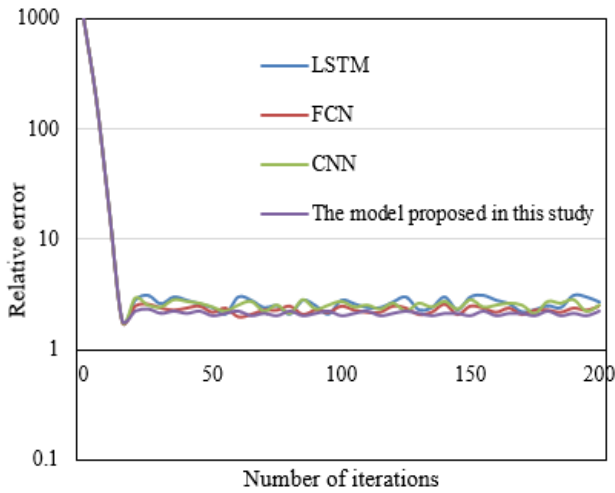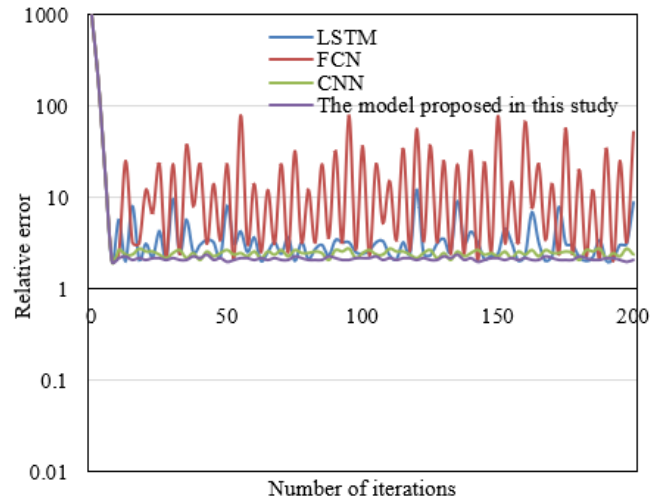

(1) Normal data
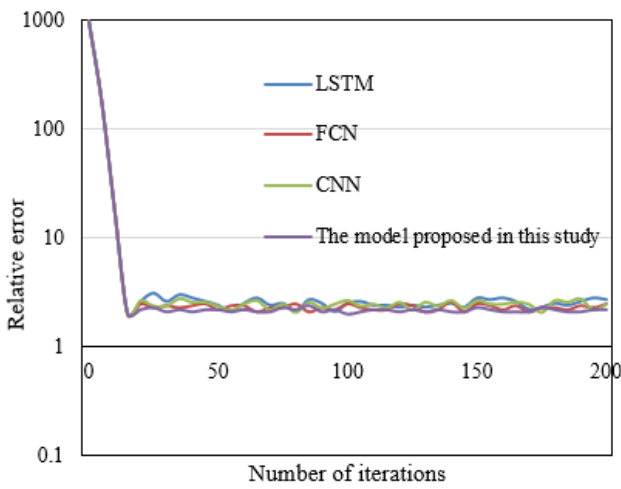
(2) Noise addition
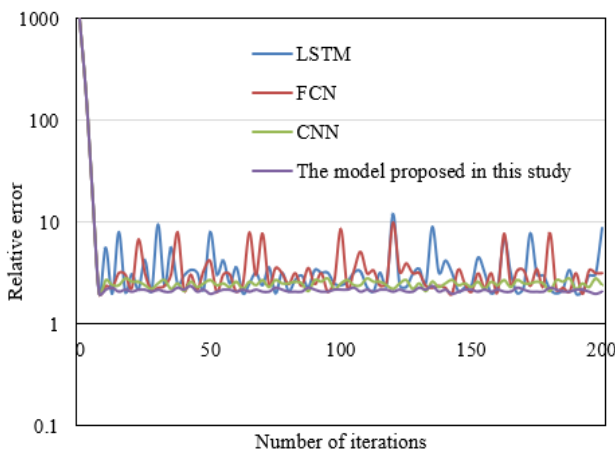
(3) Missing features

(4) Missing samples

Figure 9. Error curves of different models in thermodynamic parameter identification

5. CONCLUSION

This research initially centered on developing a one-dimensional multi-regional coupled temperature field model, with the objective of accurately identifying thermodynamic parameters through a precise representation of temperature variations across time and space. An analysis of empirical data, juxtaposed with model predictions, demonstrated that the proposed model adeptly captures the dynamic nature of temperature changes. While certain deviations were noted at specific time points, the overall predictions of the model closely aligned with actual measurements, thereby affirming its efficacy and potential for practical implementation.

Moreover, addressing the limitations of traditional methods in handling datasets with noise, missing features, and incomplete samples, a novel model integrating deep learning with rough set theory was introduced. Comparative assessments across various data conditions underscored this model's superiority, particularly in scenarios marred by compromised data integrity. This model, enhanced by the incorporation of rough set theory into deep learning frameworks, exhibited heightened stability and accuracy, especially in the context of data uncertainty and fuzziness. The experimental results, particularly the application of the fuzzy rough loss function during the training process, further corroborated the model's effectiveness. The observable decline and subsequent stabilization of the loss function value post-initialization reflected the model's rapid convergence to an optimal or near-optimal state, thereby reducing prediction errors and improving the precision of thermodynamic parameter identification.

In conclusion, the findings from this study reveal that the fusion of deep learning with rough set theory presents an effective approach for the identification and prediction of thermodynamic parameters within a one-dimensional multi-regional coupled temperature field. The integrated model not only maintains low error rates but also demonstrates robustness in various data scenarios, including those with noisy data and missing features or samples. These attributes validate both the scientific merit and the practical applicability

of the proposed approach, offering new insights and methodologies for modeling and analyzing complex systems in future endeavors.

REFERENCES

[1] Kumar, S.N., Rajabathar, J.R., Karnan, M., Kavitha, N.P. (2023). Estimation of effective diffusivity, thermodynamic parameter and drying kinetics exploration in coffee berries drying. Reaction Kinetics, Mechanisms and Catalysis, 136(3): 1371-1384. https://doi.org/10.1007/s11144-023-02412-0

[2] Erodotou, P., Voutsas, E., Sarimveis, H. (2020). A genetic algorithm approach for parameter estimation in vapour-liquid thermodynamic modelling problems. Computers & Chemical Engineering, 134: 106684. https://doi.org/10.1016/j.compchemeng.2019.106684

[3] Lapshin, V.P. (2021). Turning tool wear estimation based on the calculated parameter values of the thermodynamic subsystem of the cutting system. Materials, 14(21): 6492. https://doi.org/10.3390/ma14216492

[4] Glass, M., Mitsos, A. (2019). Parameter estimation in reactive systems subject to sufficient criteria for thermodynamic stability. Chemical Engineering Science, 197: 420-431. https://doi.org/10.1016/j.ces.2018.08.035

[5] Yu, X., Zhang, Y., Kong, L., Zhang, Y. (2018). Thermodynamic analysis and parameter estimation of a high-temperature industrial heat pump using a new binary mixture. Applied Thermal Engineering, 131: 715-723. https://doi.org/10.1016/j.applthermaleng.2017.12.039

[6] Glass, M., Djelassi, H., Mitsos, A. (2018). Parameter estimation for cubic equations of state models subject to sufficient criteria for thermodynamic stability. Chemical Engineering Science, 192: 981-992. https://doi.org/10.1016/j.ces.2018.08.033

[7] Karvonen, J., Shi, L., Cheng, B., Similä, M., Mäkynen, M., Vihma, T. (2017). Bohai Sea ice parameter estimation based on thermodynamic ice model and earth observation data. Remote Sensing, 9(3): 234. https://doi.org/10.3390/rs9030234

[8] Wang, Q., Qian, W.Q. (2011). Review of aerodynamic and aero-thermodynamic parameter estimation research for hypersonic aircraft. Journal of Experiments in Fluid Mechanics, 25(5): 99-104.

[9] Cuce, P.M., Cuce, E. (2012). A novel model of photovoltaic modules for parameter estimation and thermodynamic assessment. International Journal of Low-Carbon Technologies, 7(2): 159-165. https://doi.org/10.1093/ijlct/ctr034

[10] Lin, K., Tian, L., Zhao, Y., Zhao, C., Zhang, M., Zhou, T. (2022). Pyrolytic characteristics of fine materials from municipal solid waste using TG-FTIR, Py-GC/MS, and deep learning approach: Kinetics, thermodynamics, and gaseous products distribution. Chemosphere, 293: 133533. https://doi.org/10.1016/j.chemosphere.2022.133533

[11] Malik, H., Chaudhry, M.U., Jasinski, M. (2022). Deep learning for molecular thermodynamics. Energies, 15(24): 9344. https://doi.org/10.3390/en15249344

[12] Yin, J., Wang, F., Shankar, M.A. (2023). DeepThermo: Deep learning accelerated parallel monte carlo sampling for thermodynamics evaluation of high entropy alloys. In 2023 IEEE International Parallel and Distributed Processing Symposium (IPDPS), St. Petersburg, FL, USA, pp. 333-343. https://doi.org/10.1109/IPDPS54959.2023.00041

[13] Lapenna, M., Faglioni, F., Fioresi, R. (2023). Thermodynamics modeling of deep learning systems for a temperature based filter pruning technique. Frontiers in Physics, 11: 1145156. https://doi.org/10.3389/fphy.2023.1145156

[14] Dutta, D., Pal, S.K. (2022). Z-number-based AQI in rough set theoretic framework for interpretation of air quality for different thresholds of PM2.5 and PM10. Environmental Monitoring and Assessment, 194(9): 653. https://doi.org/10.1007/s10661-022-10325-z

[15] Hou, Z.J., Chen, H.X. (2011). Sensor drifting fault diagnosis based RS and ANN. Advanced Materials Research, 204: 1848-1851. https://doi.org/10.4028/www.scientific.net/AMR.204-210.1848

[16] Shardt, N., Elliott, J.A. (2019). Gibbsian thermodynamics of wenzel wetting (was wenzel wrong? revisited). Langmuir, 36(1): 435-446. https://doi.org/10.1021/acs.langmuir.9b02984

[17] Chtchelkatchev, N.M., Ryltsev, R.E., Magnitskaya, M.V., Gorbunov, S.M., Cherednichenko, K.A., Solozhenko, V.L., Brazhkin, V.V. (2023). Local structure, thermodynamics, and melting of boron phosphide at high pressures by deep learning-driven ab initio simulations. The Journal of Chemical Physics, 159(6). https://doi.org/10.1063/5.0165948

[18] Hernandez, Q., Badias, A., Gonzalez, D., Chinesta, F., Cueto, E. (2021). Deep learning of thermodynamics-aware reduced-order models from data. Computer Methods in Applied Mechanics and Engineering, 379: 113763. https://doi.org/10.1016/j.cma.2021.113763

[19] Sohl-Dickstein, J., Weiss, E., Maheswaranathan, N., Ganguli, S. (2015). Deep unsupervised learning using nonequilibrium thermodynamics. In International Conference on Machine Learning. PMLR, pp. 2256-2265.

[20] Long, J., Hyder, M.N., Huang, R.Y.M., Chen, P. (2005). Thermodynamic modeling of contact angles on rough, heterogeneous surfaces. Advances in Colloid and Interface Science, 118(1-3): 173-190. https://doi.org/10.1016/j.cis.2005.07.004

[21] Barbieri, L., Wagner, E., Hoffmann, P. (2007). Water wetting transition parameters of perfluorinated substrates with periodically distributed flat-top microscale obstacles. Langmuir, 23(4): 1723-1734. https://doi.org/10.1021/la0617964

[22] Brusseau, M.L. (2023). Determining air-water interfacial areas for the retention and transport of PFAS and other interfacially active solutes in unsaturated porous media. Science of The Total Environment, 884: 163730. https://doi.org/10.1016/j.scitotenv.2023.163730